Morphological and optical characterization of transparent thin films obtained at low temperature using ZnO nanoparticles

A. ALEXA[a], N. TIGAU[b], P. ALEXANDRU[a], A. PIMENTEL[c], R. BRANQUINHO[c], D. SALGUEIRO[c], T. CALMEIRO[c], R. MARTINS[c], E. FORTUNATO[c], V. MUSAT[a*]

[a]*Center of Nanostructures and Functional Materials- CNFM, Faculty of Engineering, "Dunărea de Jos" University of Galati, Galati, Romania*

[b] *Center of Nanostructures and Functional Materials- CNFM, Faculty of Sciences and Environment, "Dunărea de Jos" University of Galati, Galati, Romania*

[c]*CENIMAT/I3N, Departamento de Ciencia dos Materiais, Faculdade de Ciencias e Tecnologia, FCT, Universidade Nova de Lisboa (UNL), and CEMOP/UNINOVA, Caparica, Portugal*

Transparent metal oxides thin films are a class of inorganic conductors and semiconductors with significant importance for use in portable electronics, displays, flexible electronics, multi-functional windows and solar cells. Due to the recent development of transparent and flexible electronics, there is a growing interest in depositing metal-oxide thin-film on plastic substrates that can offer flexibility, lighter weight, and potentially lead to cheaper manufacturing by allowing printing and roll-to-roll processing. The plastic substrates, however, limit device processing to below 200°C. In this context, the deposition of high-performance semiconductor thin films from dispersions of pre-prepared oxide nanoparticles at temperatures below 200°C represents a potential key route. This paper reports on the preparation of ZnO transparent thin films using solution-processed nanoparticles (NPs) precipitated from zinc acetate alcoholic solution with potassium hydroxide. The nanoparticles size distribution, microstructure and crystallinity were measured by dynamic light scattering (DLS), Fourier transform infrared spectroscopy (FTIR) and X-ray diffraction (XRD). The thin films were deposited by spin-coating onto soda lima glass substrate, using a dispersion of 1wt% ZnO NPs. The morphology of the films annealed at 120 and 180°C, observed by atomic force microscopy and cross-section scanning electron microscopy, shows columnar grains with diameter ranging between 20 and 70 nm, depending on the conditions of depositions. Optical measurements indicated high transparency, between 85 and 94 %, in the visible range, a direct nature of band-to-band transitions and band gap values between 3,22 and 3,32 eV. The refractive index and extinction coefficient have been calculated from optical transmittance and reflectance spectra.

(Received July 20, 2015; accepted September 9, 2015)

Keywords: ZnO nanoparticles, Transparent thin films, Morphology, Microstructure, Optical properties

1. Introduction

Nowadays much attention is being given to transparent and flexible electronic devices based on metal-oxide semiconductor thin-films. In the thin film transistors (TFTs), widely investigated as key component of transparent and conductive electronics [1], metal oxide films can fulfill both the function of the transparent electrode (TCO) and the function of semiconductor channel. Transparent conductive oxides (TCO) combine simultaneously a high electrical conductivity with high optical transparency in visible spectra and have been widely used in a variety of applications (e.g. antistatic coatings, touch display panels, solar cells, flat panel displays, heaters, defrosters, optical coatings, among others) [2].

A number of metal oxides films have been introduced into the construction of TFT devices, demonstrating good electrical properties such as carrier concentration, mobility and on/off ratio. For instance, SnO_2: F (FTO) films exhibits conductivity of 100–1000 $S \cdot cm^{-1}$, carrier concentration of 10^{19}–10^{20} cm^3, and carrier mobility of 5–30 cm^2 $(V \cdot s)^{-1}$[3-4]. In_2O_3 films deposited by spray pyrolysis at 400ºC have demonstrated 1450 $S \cdot cm^{-1}$ conductivity with 23–37 cm^2 $(V \cdot s)^{-1}$ carrier mobility and 10^{20} cm^{-3} carriers concentration [3]. In-doped ZnO (IZO) thin films deposed by spray pyrolysis and heating at 370°C obtained a conductivity of 345 $S \cdot cm^{-1}$ with a mobility of 12.5 cm^2 $(V \cdot s)^{-1}$ and carrier concentration of $1.7 \cdot 10^{20}$ cm^3 achieved for 3 at% In [3, 5-6]. CdO–SnO_2 thin films with a conductivity of 280 $S \cdot cm^{-1}$; were obtained by spray pyrolysis at 500°C [7]. G. H. Kim *et al.* reported nanocrystalline indium-gallium zinc oxide (IGZO)-based devices with a mobility of ~1 cm^2 $(V \cdot s)^{-1}$ and on-to-off ratio of 10^6 [8-9]. Amorphous In:Ga:ZnO (1:1:1) thin films used in TFTs demonstrated an electron mobility of 10 cm^2 $(V \cdot s)^{-1}$ [2]. Al-doped ZnO thin films are considered as the most adequate to replace the more expensive indium tin oxide (ITO) thin films [1, 10-11].

Zinc oxide, classified as II-VI group semiconductor with a broad energy band (3.37 eV), high thermal and mechanical stability even at room temperature, is a very attractive material for potential use in electronics, optoelectronics and laser technology [12]. ZnO thin films annealed at 300–500°C produced TFTs with a field-effect mobility of 5-6 $cm^2 V^{-1}s^{-1}$ (that surpasses typical a-Si channel values of <1 $cm^2 V^{-1}s^{-1}$) and current on-to-off ratio of 10^5–10^6 [3].

Due to the recent development of transparent and flexible electronics, there is a growing interest in depositing thin-film metal-oxide semiconductors on plastic substrates that can offer flexibility, lighter weight, and potentially lead to cheaper manufacturing by allowing printing and roll-to-roll processing. However, the temperature of the device processing is limited to a maximum of ~80ºC for polyethylene terephthalate (PET) substrate, 150ºC in the case of polyethylene naphtalate (PEN) substrate and 300ºC for Polyimide (PI) substrate [13]. In this context, the deposition of high-performance semiconductor thin films from dispersions of pre-prepared oxide nanoparticles at temperatures below 200°C represents a potential key route.

ZnO nanoparticles (NPs) have been prepared using various methods: sol–gel techniques, supercritical precipitation, colloidal synthesis, vapor-phase oxidation, thermal vapor transport and condensation, chemical vapor deposition, micro-emulsion, spray pyrolysis, combustion method and organometallic synthesis [4-6, 14]. Subsequently, a dispersion of the particles can be obtained using suitable stabilizing agents to avoid aggregation, provide passivation, and to guarantee solubility in the desired solvent [15]. In order to obtain stable ZnO colloids, two main surface modifications of ZnO nanoparticles with polymers are developed: adsorbing polymers with functional groups on the surfaces of ZnO nanoparticles or encapsulating ZnO nanoparticles with polymers [16].

In this paper we report on the preparation of transparent zinc oxide thin films based on ZnO NPs precipitated from zinc acetate alcoholic solution with potassium hydroxide and deposited by spin-coating onto soda lima glass substrate. The morphology, optical properties of these thin films were investigated as a function of the number of the deposited layers and conditions of their deposition, i.e. deposition rate and the temperature of post-deposition annealing.

2. Experimental

2.1 Materials and synthesis of ZnO nanoparticles

Zinc acetate dehydrate (purity >98%), potassium hydroxide, methanol (purity ≥99%), 2-propanol (purity ≥99.5%), anhydrous n-hexane (purity 95%) were purchased from Sigma Aldrich and were used without further purification.

For the synthesis of ZnO NPs, two methanol solutions, A and B, were prepared by dissolving zinc acetate dehydrate and potassium hydroxide. More in detail, solution A with the concentration of 0.11M of KOH dissolved in methanol under reflux at 60°C and solution B with the concentration of 0.16M consisted of zinc acetate dehydrate. Over the solution A, solution B was added drop wise. The mixture was heated under reflux and magnetic stirring for three hours when a clear solution was obtained. This solution was cooled down to room temperature and aged for two days, followed by concentration to 60 mL. To the concentrated solution so obtained, propanol and n-hexane were added in order to precipitate ZnO NPs [17].

High-speed centrifugation (9000 rpm) was used for the separation of ZnO NPs from the mother solution, and for each centrifugation step, a washing with methanol was applied. The obtained powder was finally dried in air at 100°C.

2.2 Thin film preparation

The prepared ZnO NPs were re-dispersed in methanol and deposited as thin films by spin-coating on soda lima glass substrates using Spin-Coater WS-650SZ-8NPP AS, Laurell. Single-layer (labeled with F1 to F4 in Table 1) and three-layered thin films samples (labeled with F5 to F8 in Table 1) were deposited at 500 and 1000 rpm and annealed at 120 and 180°C, respectively.

2.3. Nanoparticles and thin films characterization

The crystalline structure of the obtained ZnO NPs was evaluated by X-ray diffraction using a PANalytical's X'Pert PRO MRD diffractometer, with a monochromatic CuK_α radiation source (wavelength 1.540598 Å). The size of the nanoparticles was measured by dynamic light scattering (DLS) using a Zetasizer Nano ZS (Malvern Instruments Ltd). Their morphology was observed with a Zeiss Auriga scanning electron microscope. The samples preparation consisted of dispersing the nanoparticles in methanol and then depositing drops of this dispersion on the surface of a conductive carbon strip; after solvent evaporation in air, a solid thin layer of nanoparticles resulted. The cross-section morphology and thickness of the deposited thin films was observed and measured using a CrossBeam Workstation (*SEM*-FIB) – Zeiss Auriga. The films thickness was also checked by means of MII-4 interference microscope (type Linnik) with an error not exceeding 0.01 μm, using multiple-beam Fizeau fringe method [18].

The Atomic Force Microscopy (AFM) was used to investigate the topography of the surface of thin films, in ambient conditions with Asylum Research MFP-3D Standalone microscope operating in contact mode. The sample scanning was performed with a commercial Pt probes (Nanoworld ContPt). The root mean square roughness (Rms) values were evaluated with Gwyddion software.

The optical transmission and reflectance spectra were acquired at room temperature with a Perkin Elmer (Lambda 35) UV-VIS-NIR spectrophotometer, operated in air, at normal incidence, in the 200–1100 nm spectral

range. The optical band gap energy, E_g, was estimated from the fundamental absorption edge of the nanoparticles-based thin films, assuming a direct transition between valence and conduction band. The values of optical band gap were determined from the dependency of absorption coefficient, α, on the photon energy, $h\nu$, given by the equation (1):

$$(\alpha h\nu)^2 = A(h\nu - E_g) \quad (1)$$

where A is a parameter that depends on the transition probability [19]. The absorption coefficient, α, was calculated by equation (2):

$$\alpha = \frac{1}{d}\ln\left[\frac{(1-R)^2 + \sqrt{(1-R)^2 + 4R^2T^2}}{2T}\right], \quad (2)$$

where d is the film thickness, T and R are the transmittance and reflectance, respectively, of the investigated samples [20].

The films refractive index, n, was calculated according to the equation:

$$n = \frac{R+1}{R-1} + \left[\left(\frac{R+1}{R-1}\right)^2 - (1-k^2)\right]^{\frac{1}{2}}, \quad (3)$$

where k is the extinction coefficient, calulated as such:

$$k = \frac{\alpha\lambda}{4\pi}, \quad (4)$$

where λ represents the wavelength.

3. Results and Discussion

3.1. Morpho-structural characterization

The chemical reactions of zinc oxide production using zinc acetate and potassium hydroxide usually consist in the formation of zinc (II) hydroxide (Eq. 5) followed by water elimination through self-condensation of zinc (II) hydroxide molecules (Eq. 6).

$$Zn(CH_3COO)_2 + 2KOH \rightarrow Zn(OH)_2 + 2CH_3COOK \quad (5)$$

$$Zn(OH)_2 \rightarrow ZnO + H_2O \quad (6)$$

DLS measurements of nanoparticles present in the solution at the end of the synthesis (after two hours of ageing) and after separation, washing and redispersion in methanol (Figure 1), shows particles sizes within narrow ranges of 3.5 to 8 nm (with mean particle size of about 5.7 nm) and of 7.5 to 20 nm (with mean particle size of about 12 nm), respectively.

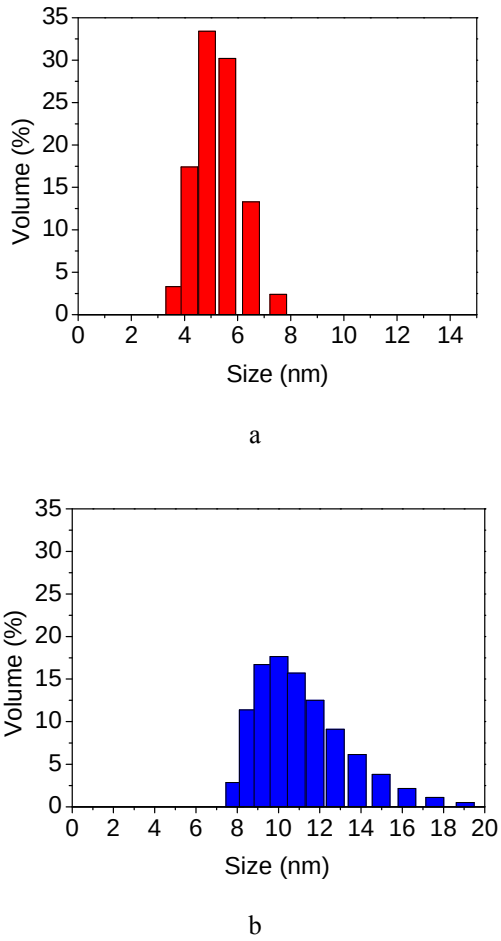

Fig. 1. DLS histograms of as-prepared (two hours aged) ZnO NPs in mother solution (a) and after separation, washing and re-dispersing in methanol (b).

The XRD pattern (Fig. 2a) confirms the wurtzite type pure phase of zinc oxide, with the three main diffraction peaks located at 31.9, 34.3, 36.2° 2θ, that are assigned to (100), (002) and (101), respectively. The other diffraction peaks corresponds to (102), (110) and (103) planes of the wurzite pattern of ZnO. The average crystallite size (L) of ZnO NPs was calculated based on Debye-Scherrer's equation $B(2\theta) = (K\cdot\lambda)/(L\cdot\cos\theta)$, where B is the full width at half the maximum intensity (FWHM), λ is the X-ray wavelength, θ is the diffraction angle and K is the Scherrer's constant whose value for spherical particles is 0.89 [17]. The calculated ZnO crystallite size was found to be about 11 nm, in a very close agreement with the value estimated from LDS data, which means that the nanoparticles measured by LDS are ZnO single crystals.

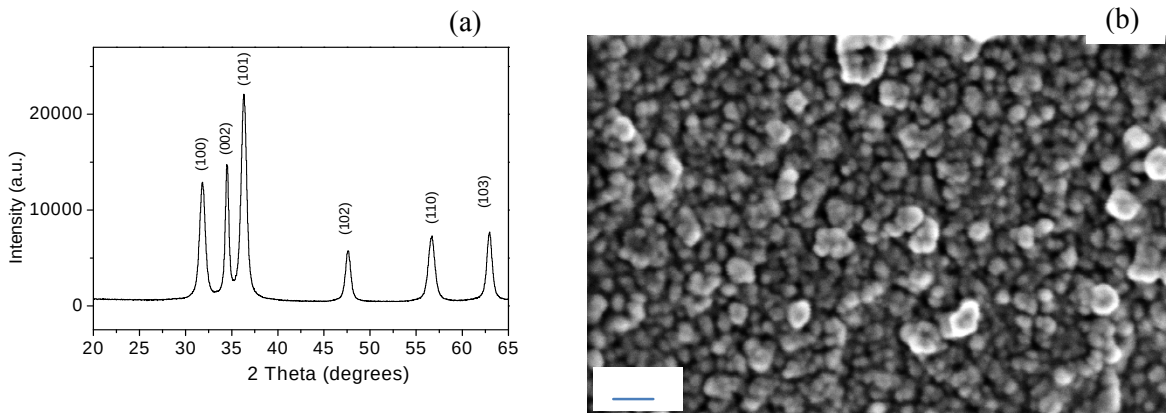

Fig. 2. XRD pattern (a) and SEM image (b) of the prepared ZnO NPs

The particles size and the morphology of the prepared ZnO NPs studied by scanning electron microscopy (SEM) are given in Fig. 2b. The SEM image of ZnO NPs resulted from the alcoolic dispersion after solvent evaporation shows larger range size agglomerates of ZnO single crystals, in the range of 10-50 nm, with nearly spherical shape.

The cross-section morphology and thickness of the deposed thin films observed by *SEM*-FIB technique are shown in Fig 3 and Table 1.

The thickness increases with the number of layers and decreases with increasing the annealing temperature. One can notice a certain proportion between the number of deposed layers and the film thickness, that ranges between 200-300 nm and 540-890 nm for single-layer and three-layers samples, respectively.

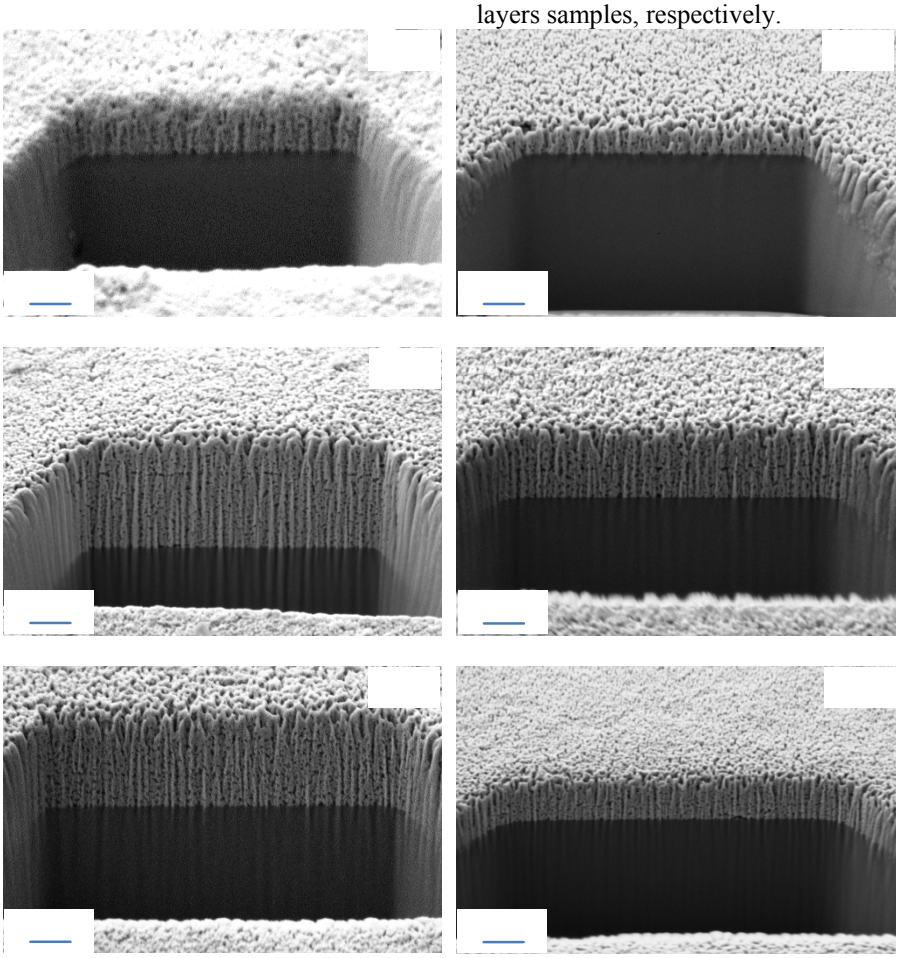

Fig. 3. SEM-FIB cross-section micrographs of ZnO NPs-based thin films.

Table 1. Experimental deposition parameters and some characteristics of the investigated films

Sample symbol	Number of layers	Deposition rate (rpm)	Annealing temperature (°C)	Film thickness (nm)	E_g (eV)	*Rms* (nm)
F1	1	500	120	285	3.278	3.88
F2			180	205	3.226	3.33
F3		1000	120	164	3.284	4.11
F4			180	122	3.262	3.72
F5	3	500	120	880	3.313	4.85
F6			180	570	3.274	5.33
F7		1000	120	730	3.323	4.62
F8			180	520	3.316	5.25

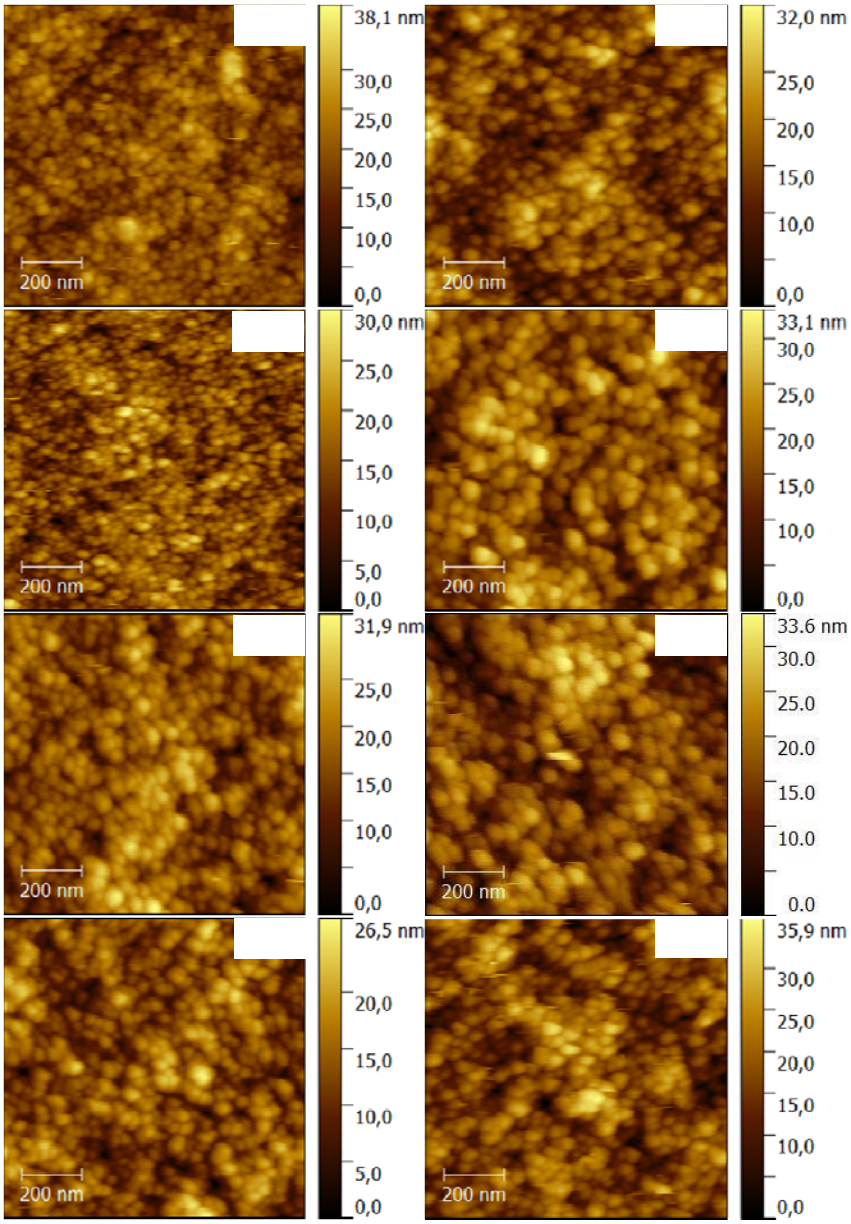

Fig. 4. AFM images of ZnO NPs-based thin films.

Columnar grains with a relatively compact and homogeneous distribution by size and shape regardless of deposition rate and the post deposition thermal treatment can be observed from Figure 3. More relevant for the size of the diameter of the columnar grain are the atomic force microscopy images (Figure 4) that show roundish grains

with diameters between 20 and 60 nm. Some porosity can be observed, which is higher for one-layer films than for three-layers ones and slightly increases with increasing the annealing temperature from 120 to 180°C. The mean surface roughness (*Rms*) of the films, calculated from atomic force microscopy measurements, is small, varying between 3.33 and 5.33 nm as a function of the spin deposition speed, number of layers and annealing temperature. *Rms* increases with the number of layers and the films thickness. For the three-layered films (F5-F8) the surface roughness increases with increasing annealing temperature, but an opposite effect can be observed for single-layer films (F1-F4) (Table 1, Fig 4).

3.2. Optical properties

The optical transmittance and reflectance spectra in the UV-Vis-NIR wavelength region (200-1100 nm) of the investigated thin films are shown in Fig. 5. All these films, with different thicknesses, ranging from about 160 to about 900 nm, show excellent optical transmittance in the visible range with values between 85 and 94% and low reflectance values between 5 and 10% in the visible domain. As expected, the decrease of the film thickness is accounted for the increase of transmittance in the visible domain.

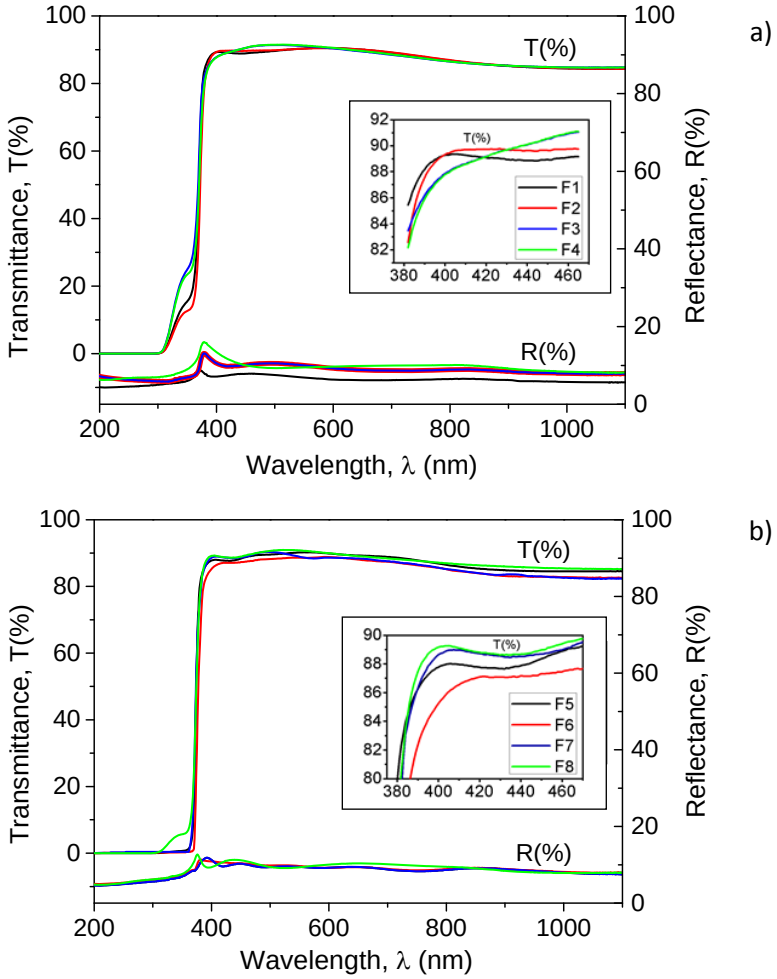

Fig. 5. Optical transmittance and reflectance spectra for single-layer (a) and for three-layers samples (b).

From Fig. 5 (a), one can notice that for the single-layer thin films (F1- F4) the values of transmittance range between 86.4 and 91.5%. At the fundamental absorption interval (300- 375 nm), one can observe that higher transmittance values are attained for the thicker one-layer films obtained at lower spin-coating rate (F1 and F2 in the detail of Fig 5(a). From Fig. 5 (b) showing the transmittance and reflectance optical spectra of the three-layers thin films (F5- F8), one can notice that the values of transmittance are slightly lower, between 85.2 and 90.9%.

At the fundamental absorption interval (300–375 nm), one can observe higher transmittance values for the three-layers films obtained at higher spin-coating rate (F7 and F8 in the detail of Fig 5b). In the UV side of the spectra, a „flattening" of the fundamental absorption occurs in most of the three-layers thin films.

The calculation of the optical band gap (*Eg*) from the variation of the absorption coefficient, α, vs the photon energy, $h\nu$, is presented in Fig. 6.

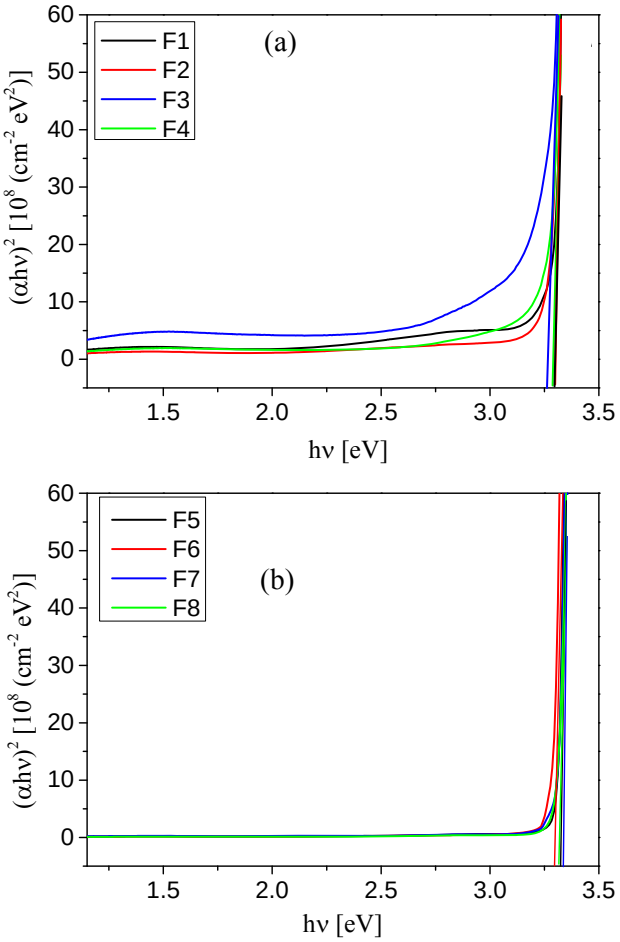

Fig. 6. αhν vs hν curves of the single-layer (a) and three-layers samples (b).

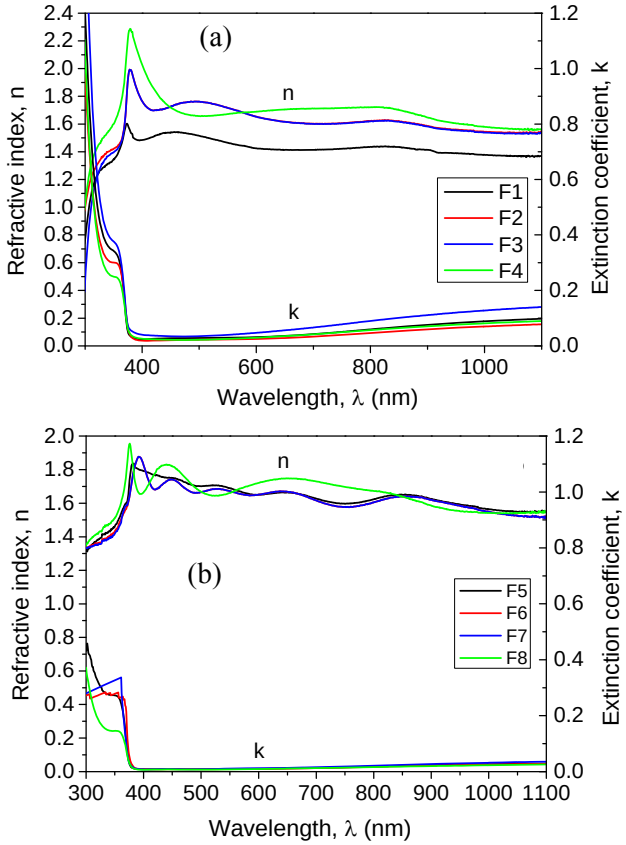

Fig. 7. The variation of refractive index and extinction coefficient for one layer samples (A) and three layered samples (B).

The obtained values of the optical band gap for the investigated thin films are presented in Table 1. These values range between 3.226 and 3.323 eV. From Table 1, one can notice that higher film thickness leads to higher *Eg* values and higher post-deposition annealing temperature leads to lower *Eg* values. The three-layered films show an increase of about 0,035 eV with respect of the thinner one-layer films, which is very close to the band gap of intrinsic ZnO powder [21-22]. The samples annealed at 180°C (F2, F6) show a lowering with about 0.050 and 0.040 eV, respectively, of the *Eg* values, with respect to the corresponding samples (F1, F5) annealed at 120°C.

The variations of the refractive index (n) and the extinction coefficient (k) in the wavelength region of 300–1100 nm are shown in Fig. 7. The decrease of the refractive index is attributed to the decrease of thickness of the films. The refractive index of thin films have shown the normal dispersion in the visible range.

The effect of the spin rate and the annealed temperature on the values of the refractive index (*n*) is stronger in the case of thinner single-layer films (F1-F4) than for the thicker films with three layers (F5-F8), whose curves of variation with lambda are much closer, which can be due to increase of the compaction of thicker films. So, for the films with one and three layers, *n* values varies between 2.3-1.4 and 1.95-1.55, respectively. These values strongly recommend their use in transparent electronic applications.

4. Conclusions

ZnO single nanocrystals with a mean diameter of about 5.7 nm in mother solution and 12 nm after re-dispersing in methanol, synthesized from zinc acetate dehydrate $Zn(CH_3COO)_2{:}2H_2O$ in the presence of potassium hydroxide KOH, were used for the preparation of ZnO transparent thin films.

The thin films deposited by spin-coating onto soda lima glass substrate, using a dispersion of 1wt% ZnO NPs, and annealed at 120 and 180°C shows columnar grains with diameter ranging between 20 and 70 nm and a wurtzite type pure phase zinc oxide.

All the obtained films, with one and three-layers show thickness ranging from about 160 to 890 nm, excellent optical transmittance in the visible range with values between 85 and 94%, low reflectance values between 5 and 10% in the visible domain and band gap values between 3,22 and 3,32 eV. These values, together with values of the refractive index and extinction coefficient calculated from optical transmittance and reflectance spectra, recommend the obtained films for use in transparent electronic applications.

Acknowledgements

The work of Alexandru Alexa has been funded by the Sectoral Operational Programme Human Resources Development 2007-2013 of the Ministry of European Funds through the Financial Agreement POSDRU/159/1.5/S/132397.

The project PN-II-PT-PCCA Contract Nr. 27/2014 - NANZON is also acknowledged.

References

[1] E. Fortunato, P. Barquinha, R. Martins, Adv. Mater. **24**, 2945 (2012).
[2] D., Ginley, H., Hosono, D. C. Paine, Handbook of transparent conductors, Springer, New York, 2010, e-ISBN 978-1-4419-1638-9.
[3] R. M. Pasquarelli, D.S. Ginley, R. O'Hayre, Chem. Soc. Rev., **40**, 5406 (2011).
[4] J.C. Fan, K.M., Sreekanth, Z. Xie, S.L. Chang, K.V., Rao, Progress in Materials Science, **58**, 874 (2013).
[5] Y. H. Kang, S. Jeong, J. Min Ko, Ji-Yo, Lee, Y. Choi, C. Lee, S.Y. Cho, Journal of Materials Chemistry C **2**, 4247 (2014).
[6] T. Schneller, R. Waser, M. Kosec, D. Payne, Chemical Solution Deposition of Functional Oxide Thin Films, Springer, New York, 2013, ISBN 978-3-211-99311-8.
[7] V., Krishnakumar, K., Ramamurthi, Kumaravel, K., Santhakumar, Curr. Appl. Phys, **9**, 467 (2009).
[8] G.H. Kim, H.S. Shin, B.D. Ahn, K.H. Kim, W.J. Park, H.J. Kim, J. Electrochem. Soc. **156**, H7 (2009).
[9] C. Jagadish, S.J. Pearton, Zinc oxide bulk, thin films and nanostructures. Processing, Proprieties and Applications, Elsevier, 2006.
[10] P. Prepelita, C. Baban, F. Iacomi, J. Optoelectron. Adv. Mater. **9**(7), 2166 (2007).
[11] V. Musat, B. Teixeira, E. Fortunato, R. C. C. Monteiro, Thin Solid Films, **502,** 219 (2006).
[12] A. Kołodziejczak-Radzimska, T. Jesionowski, Materials, **7**, 2833 (2014).
[13] A. Facchetti, T.J. Marks, Transparent electronics: From synthesis to Applications, Wiley, 2010, ISBN 978-0-99077-3.
[14] Y.S. Rim, H.S. Lim, H.J. Kim, ACS Appl. Mater. Interfaces, **5**, 3565 (2013).
[15] K. Zilberberg, J. Meyerb, T. Riedl, J. Mater. Chem, **1**, 4796 (2013).
[16] C. Li, Y. Li, Y. Wu, B.S. Ong, R.O. Loutfy, Journal of Applied Physics, **102**, 076101 (2007).
[17] D. Costenaro, F. Carniato, G. Gatti, L. Marchesea, C. Bisio, Preparation of Luminescent ZnO Nanoparticles Modified with Aminopropyltriethoxy Silane for Optoelectronic Applications, The Royal Society of Chemistry, doi: 10.1039/c0xx00000x
[18] K.L. Chopra, Thin Film Phenomena, McGraw-Hill, New York, 1969
[19] A. AlKahlout, J Sol-Gel Sci Technol, **67**, 331 (2013).
[20] N. Ghraïri, F. Aousgi, M. Zribi, M. Kanzari, Chalcogenide Letters, **7**(3), 217 (2010).
[21] H.L. Hartnagel, A.L. Dawar, A.K. Jain, C. Jagadish, Semiconducting Transparent Thin Films, Institute of Physics Publishing, Bristol/PA, 1995.
[22] J.I. Pankove, Optical Progress in Semiconductors, Dover, New York, 1975.

*Corresponding author : Viorica.Musat@ugal.ro